Optics Letters

# Two-pole microring weight banks

Alexander N. Tait,[1,*] Allie X. Wu,[1,2] Thomas Ferreira de Lima,[1] Mitchell A. Nahmias,[1] Bhavin J. Shastri,[1] and Paul R. Prucnal[1]

[1]Lightwave Communications Research Laboratory, Department of Electrical Engineering, Princeton University, Princeton, New Jersey 08544, USA
[2]General Dynamics Corporation, Mount Laurel, New Jersey 08054, USA
*Corresponding author: atait@princeton.edu

Received 29 January 2018; revised 5 April 2018; accepted 7 April 2018; posted 11 April 2018 (Doc. ID 319497); published 7 May 2018

**Weighted addition is an elemental multi-input to single-output operation that can be implemented with high-performance photonic devices. Microring (MRR) weight banks bring programmable weighted addition to silicon photonics. Prior work showed that their channel limits are affected by coherent inter-channel effects that occur uniquely in weight banks. We fabricate two-pole designs that exploit this inter-channel interference in a way that is robust to dynamic tuning and fabrication variation. Scaling analysis predicts a channel count improvement of 3.4-fold, which is substantially greater than predicted by incoherent analysis used in conventional MRR devices. Advances in weight bank design expand the potential of reconfigurable analog photonic networks and multivariate microwave photonics.** 

***OCIS codes:*** (250.5300) Photonic integrated circuits; (070.1170) Analog optical signal processing; (130.7408) Wavelength filtering devices; (200.4860) Optical vector-matrix systems.

https://doi.org/10.1364/OL.43.002276

Next-generation radio systems call for signal processing approaches that are significantly broader bandwidth and more energy efficient than digital signal processing [1]. Photonic technologies excel at high-bandwidth analog signal processing, and the silicon photonics industry could make these types of processors manufacturable [2]. Integrated microwave (i.e., analog) photonics has offered improvements for programmable filters [3,4], interference suppression [5,6], and waveform generation [7], all of which are single-input, single-output functions. An important multi-input, single-output operation is weighted addition, also known as a vector dot product or multiply-accumulate. Photonic weighted addition has been explored for use in more advanced processors, including multivariate radio-frequency photonics [8–10] and photonic neural networks [11,12]. Addition occurs through the photodetection of mutually incoherent wavelength-division multiplexed (WDM) optical carriers, and weighting is performed by a tunable spectral filter called a photonic weight bank.

Microring (MRR) weight banks bring photonic weighted addition to silicon photonics [13]. In a MRR weight bank, the transmission seen by a WDM channel is configured by thermally tuning that filter on and off resonance [14]. A bank of these filters coupled to two-bus waveguides (WGs), shown in Fig. 1(a), independently weights all WDM channels [15]. A complementary −1 to +1 weight range is achieved by balanced photodetection of the multiplexed bus WGs. The channel count is limited by a resonator-free spectral range (FSR) and the bank's ability to independently weight neighboring WDM channels [16]. This Letter extends this limit, expanding on a procedure developed in Ref. [17].

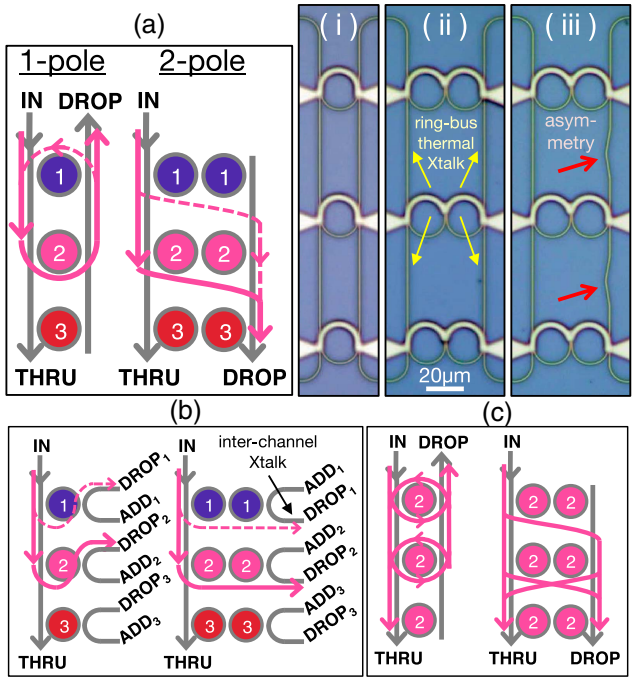


**Fig. 1.** (a) Coherent paths are resonator-like in 1-pole weight banks and interferometer-like in 2-pole weight banks. The pink lines are optical paths taken by the $\lambda_2$ signal; the solid line is through the nominal filter; and the dashed lines are through a neighboring filter. Device (i), 1-pole weight bank; devices (ii, iii), 2-pole weight banks with thermal Xtalk to bus WGs (yellow arrows). Device (iii) contains a bus length asymmetry (red arrows). (b) Conventional demultiplexer with incoherent inter-channel Xtalk. (c) Conventional SCISSOR/ladder filter where all parallel-coupled rings act on a single wavelength carrier.

Prior research in MRR circuits has focused on single-bus, multi-wavelength MRR devices [Fig. 1(b)], such as demultiplexers [18,19]. In demultiplexers, a WDM channel partially coupled through a neighboring filter exits the wrong output port, resulting in inter-channel cross-talk (Xtalk), which limits minimum channel spacing [20,21]. Extensive research has also been directed towards double-bus, single-wavelength MRR devices [Fig. 1(c)], including series/parallel-coupled ladders [22,23], 1-pole and 2-pole (a.k.a. twisted) SCISSORs [24–26], and more generalized circuits [27,28]. In these cases, all MRRs within a filter act on a single wavelength channel, each resonating at or near a common wavelength. These single-wavelength filters are often used within demultiplexers, in which case subsequent channel filters (each containing multiple MRRs) are cascaded via a single bus WG.

In a MRR weight bank, parallel-coupled 1- or 2-ring filters act on different WDM carriers. In this respect, they are similar to demultiplexers; however, unlike demultiplexers, a weight bank does not separate WDM channels into individual WGs. A WDM channel partially coupled through a neighboring filter exits the same two output ports. This crucial difference results in (1) the breakdown of inter-channel Xtalk as a meaningful concept and (2) the presence of two-bus WGs between filters that act upon different WDM channels. The minimum channel spacing is limited by the ability to weight neighboring channels independently, rather than inter-channel Xtalk [16]. Furthermore, the path taken through the neighboring filter interferes coherently with the path taken through the nominal filter. This coherent phenomenon has a pronounced impact on channel density limits.

The nature of inter-filter interference is fundamentally different for MRR filters that are odd-pole vs. even-pole because signals are dropped in opposite directions [Fig. 1(a)]. The number of poles is equal to the number of series-coupled MRRs per channel filter. In an odd-pole bank, a channel partially coupled through a neighboring filter returns through the opposite bus WG to complete a resonator-like feedback path. In an even-pole bank, the partially dropped channel continues in the same direction to complete an interferometer-like feed-forward path instead. Interferometer-like interference depends on a path length difference, rather than a sum, so changes that affect both bus WGs equally will not change the interferometric phase condition. While the group velocity of WGs as fabricated varies significantly over the chip area, this variation is spatially correlated [29,30]. Dynamic variation due to thermal tuning can be made congruent using the designs introduced in this Letter.

In this Letter, we demonstrate that the inter-channel phase condition is tolerant to dynamic tuning only in 2-pole weight banks. Furthermore, we show that 2-pole banks can be tailored to exploit this effect for deeper isolation between channels, even in the presence of fabrication variation. Using the parametric scaling analysis developed in Ref. [16], we estimate that these properties represent a 3.4× improvement in channel scalability.

Three silicon MRR weight banks, pictured in Fig. 1(i, ii, and iii), are fabricated to study inter-filter effects: type (i) is a 1-pole bank; type (ii) is a 2-pole bank with identical bus WGs; and type (iii) is a 2-pole bank with a bus WG asymmetry. A bus length asymmetry of 95 nm is designed to give a $\pi/2$ phase shift, given the TE group index of $n_g = 4.2$ on this platform [31] ($\Delta\phi = 2\pi n_g \cdot 95\ \text{nm}/\lambda_0$). Heating filaments provide independent resonance control and indirectly heat the bus WGs. The indirect MRR-to-bus thermal Xtalk (different from inter-channel signal Xtalk) is desirable in this experiment as a way to effect bus WG index shifts. Filament symmetry is critical to ensure that index shifts are applied equally to both MRRs within a 2-pole filter and both surrounding bus WGs. A 1-pole bank with bus length asymmetry is not fabricated because it is expected to behave the same as device (i).

Silicon-on-insulator samples have a silicon thickness of 220 nm and a width of 500 nm with fully etched WGs, a 3 μm oxide passivation layer, a Ti/Au heating filament layer, and an Al routing layer [32]. The measured WG loss is 7 dB/cm for the TE mode. In each bank, the MRRs have a short 2 μm straight coupling region with arcs of slightly different radii near 10 μm. Exact layout perimeters are $L = [68.0, 68.1, 68.2]\mu\text{m}$. This design is intended for approximately equal FSRs of 9.1 nm and inter-channel resonance offsets of 2.3 nm. The actual offset is affected by fabrication variation. These 1- or 2-pole MRR channels are arranged in a parallel add/drop configuration with symmetric bus coupling gaps of 100 nm. The MRRs in each 2-pole filter are separated by a gap of 300 nm, optimized to critically couple the two MRRs. The critical coupling gap was determined from a previous chip generation (not shown). The sample is mounted on a temperature-controlled alignment stage and coupled to fiber through focusing sub-wavelength grating couplers [33]. During the experiment, the heating filaments are driven by computer-controlled current sources, while the device drop port is monitored by an optical transmission spectrum analyzer (Apex AP2440A) [Fig. 2(a)]. Based on measurements, the sheet resistivity of routing layers, and the probe and via resistances, we estimate an internal filament resistance of 52Ω. The measured thermal tuning efficiency is then 0.22 nm/mW, in other words, an FSR power of $P_{\text{FSR}}[\text{mW}] = 42$ mW.

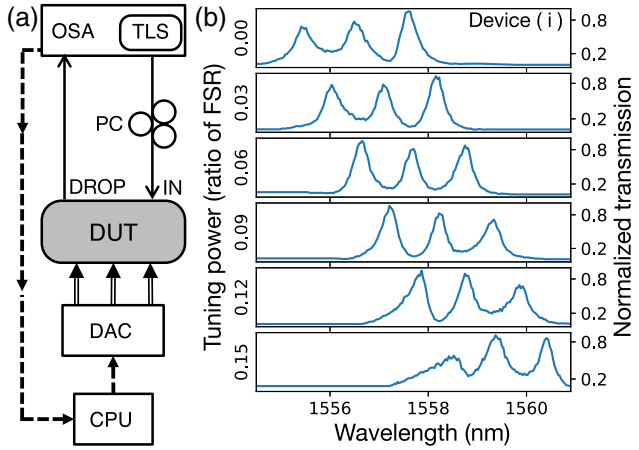


**Fig. 2.** Experimental setup and tuning procedure. (a) Optical drop transmission and electrical probing setup of a device under test (DUT). OSA, optical spectrum analyzer; TLS, tunable laser source; PC, polarization controller; DAC, digital-to-analog converter; CPU, computer controller. (b) Transmission spectra measured during the collective tuning procedure for device (i). Three resonances are tracked to a spacing of 1.0 nm and then swept in concert over a common-mode 3.0 nm, maintaining their relative spacing.

Each bank is subjected to an identical test procedure formulated to isolate the effect of the bus path length. We employ thermal Xtalk from MRR filaments to bus WGs to affect bus WG index changes. By then removing net effects on MRR WGs (i.e., wavelength shifts), we can isolate the effects on bus WGs. Initially, the resonances are independently tracked to a spacing of 1.0 nm using a peak picker and proportional control rule. Starting from this baseline point, the heater power on all filaments is increased in concert from 0.00–$0.15P_{\mathrm{FSR}}$ each. This step is shown in Fig. 2(b). Since the additional heat is equal on each MRR filter, resonance wavelengths maintain a constant separation of 1.0 nm, while the collection of peaks traverses 3.0 nm. The common-mode peak shifts are removed in Fig. 3 by re-centering each spectrum around the middle peak. Some heat generated by the MRR filaments reaches the bus WGs, an effect that remains visible after re-centering.

Figure 3 shows the results of tracking and tuning devices (i, ii, and iii) after re-centering. The *inter*-filter coherent effects of interest are observed in the dips (a.k.a. troughs) between peaks: wavelengths that partially couple to two neighboring filters. For device (i) (green), the trough profile and depth (5–13 dB) vary strongly as a function of bus path length shifts. The 2-pole devices (ii) (blue) and (iii) (red) maintain stable trough profiles, indicating that they are tolerant to dynamic tuning. Device (ii) trough minima are 10–12 dB. Device (iii) exhibits deeper isolation having trough minima of 17–19 dB. This result indicates that lithographically defined bus asymmetry (here, 95 nm) is successful at exploiting inter-channel interference, even in the face of fabrication variation.

Filter passbands exhibit non-idealities that can be attributed to *intra*-filter effects affecting the wavelengths that pass predominantly through one series-coupled filter. Some 2-pole passbands exhibit 6 dB excess loss due to slight, but non-negligible, resonance offsets [29,30]. This could be addressed with fabrication insensitive MRRs [34] or lithographic techniques tailored for multi-pole MRR filters [35]. In some cases, the passband amplitude varies with common-mode tuning. This effect is likely due to a temperature-dependent central coupling coefficient. This may be avoided by moving the middle section of the filaments away from the central gap, at the expense of tuning efficiency.

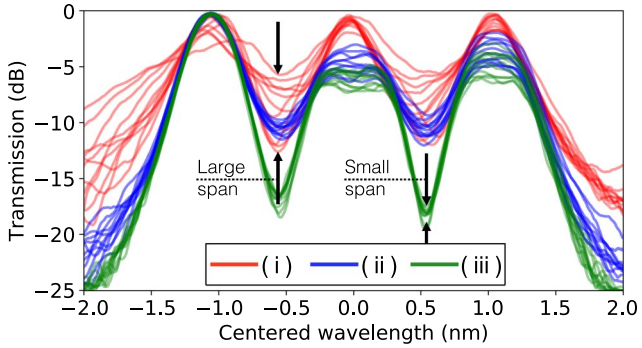


**Fig. 3.** Relative transmission data measured during the tuning procedure. The x-axis shows relative wavelength offset from the center of the profile as it is tuned. The 1-pole device (i) (red) varies strongly with common-mode tuning, while 2-pole devices (ii, iii) retain a constant profile. Furthermore, device (iii) (green) exhibits a deeper dip between peaks, indicating improved channel isolation as a result of its bus length asymmetry.

In Ref. [16], we introduced a power penalty metric that quantifies the ability to set WDM channel weights independently, as well as a procedure through which it is related to channel spacing, $\delta\omega$, and the bus optical phase. The procedure is (1) construct a model specified by MRR bank properties and WDM channel spacing; (2) simulate transmission at channel wavelengths over all possible 2D tuning states; (3) compute the conforming boundary of all possible 2D weight states; (4) compute the largest zero-centered square inscribed by the boundary. The power penalty is the side length of this square. This procedure is illustrated for a 1-pole bank in Fig. 6 of Ref. [16]. This prior work did not study the effects of MRR-to-bus thermal Xtalk or fabrication variation, assuming that the bus phase condition was fixed with tuning and able to be optimized by fabrication. We have shown here that these assumptions of a fixed bus WG phase are unrealistic for 1-pole banks and valid for 2-pole banks.

We repeat the scaling analysis procedure for 2-pole MRR weight banks using a range of channel spacings from 1 to 7 linewidths and bus (total/differential) phases from 0 to $2\pi$ to produce Fig. 4. In both 1- and 2-pole models, the bus power coupling ratio is $t_b^2 = 0.1$. In the 2-pole model, the central coupling ratio is chosen to achieve critical coupling ($t_c^2 = 0.0015$), which is favorable in all cases of interest. The minimum channel spacing, allowing for a 3 dB penalty, was found to be between $3.04 < \delta\omega_{3\,\mathrm{dB}} < 4.12$ (1-pole) and $1.20 < \delta\omega_{3\,\mathrm{dB}} < 1.75$ (2-pole). In both cases, the value depends on the bus phase. The experimental results of this Letter show that, with 1-pole banks, the round-trip bus phase changes dynamically, so the worst-case scenario must be assumed. They also showed that 2-pole banks can be fabricated with best-case performance, tolerant to dynamic tuning. Therefore, the 2-pole weight bank design potentially represents a factor of 3.4× improvement in channel density over the 1-pole device. On the platform used in this Letter, resonator $Q$-factors typically fall

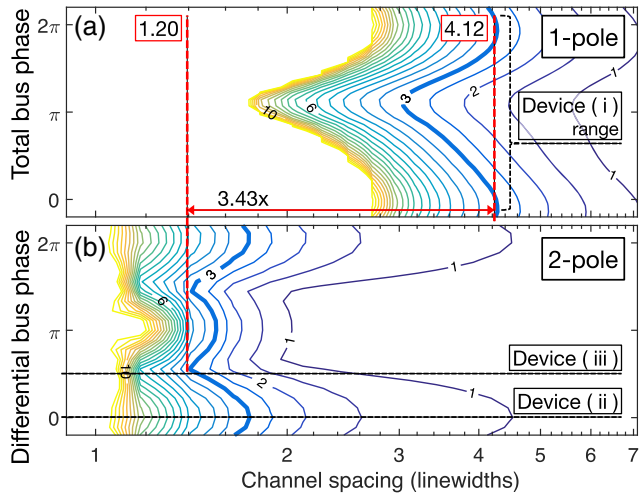


**Fig. 4.** Cross-weight insertion loss in (a) 1-pole and (b) 2-pole weight banks. Adjacent channels become more difficult to weight independently when they are spaced more closely, relative to the filter linewidth. 2-pole filters can support denser spacing because of their steeper roll-off and exploitation of inter-channel interference.

within 10k–20k with an FSR of 9.1 nm (finesse, $\mathcal{F} \approx 133$), so it could potentially yield MRR weight bank channel limits of 32 (1-pole) and 110 (2-pole).

The performance gain represented by designing 2-pole versus 1-pole filters in MRR weight banks is unexpectedly high compared to the same design change in conventional MRR demultiplexers. This means the MRR weight bank's inter-channel interference effects can be exploited, not just tolerated. In both types of devices, the steeper roll-off of the 2-pole filter allows for denser channel spacing. This impact is expected. In demultiplexers, it represents a 70% channel density improvement [20]. However, in this Letter, we calculate the corresponding improvement in MRR weight banks to be 240%. This discrepancy is achieved by exploiting inter-channel interference within the two-bus circuit.

This Letter calls for further study in weight bank control strategies. Feedforward control techniques have been shown [15], but only in the coarse WDM regime where each channel is affected by only one MRR filter. With dense WDM, this assumption is violated, so the approach would have to also model inter-filter interference, as well as variable ring-to-bus thermal Xtalk. The repeatability of 2-pole weight bank spectra hint at simplified algorithms for dense WDM weight control. We have shown here that the bus phase condition does not change with tuning, so, for example, it could be considered a fixed parameter, rather than a tuning-dependent variable.

We have compared in experiment 1-pole and 2-pole silicon MRR weight banks. As opposed to other WDM devices based on MRRs, weight banks are sensitive to coherent interactions between neighboring filters, and the character of this interaction is fundamentally different for odd-pole and even-pole filters. By tuning banks of three weights together to effectively sweep their inter-channel interferometric phase conditions, we have shown that 1-pole weight banks are not tolerant to tuning-related thermal Xtalk, while 2-pole weight banks are tolerant. The coherent inter-channel effects in 2-pole banks can be exploited for greater isolation between channels. A bus length asymmetry (here, 95 nm), designed lithographically and robust to fabrication variations, was seen to increase isolation by 5 dB. This isolation translates to a channel density increase over baseline designs, found here to be 3.4×. Channel count improvements in MRR weight banks directly impact proposed analog signal processing approaches in silicon photonics, particularly neuromorphic photonics and multivariate photonics.

**Funding.** National Science Foundation Enhancing Access to the Radio Spectrum, Directorate for Engineering (ENG) (1642991); Natural Sciences and Engineering Research Council of Canada (NSERC).

**Acknowledgment.** Fabrication support was provided by the NSERC Silicon Electronic-Photonic Integrated Circuits (SiEPIC) Program. Devices were fabricated by Cameron Horvath at Applied Nanotools, Inc., Alberta, Canada [32].

## REFERENCES

1. E. Dahlman, G. Mildh, S. Parkvall, J. Peisa, J. Sachs, Y. Selén, and J. Sköld, IEEE Commun. Mag. **52**, 42 (2014).
2. M. Hochberg, N. C. Harris, R. Ding, Y. Zhang, A. Novack, Z. Xuan, and T. Baehr-Jones, IEEE Solid-State Circuits Mag. **5**, 48 (2013).
3. L. Zhuang, C. G. H. Roeloffzen, M. Hoekman, K.-J. Boller, and A. J. Lowery, Optica **2**, 854 (2015).
4. D. Pérez, I. Gasulla, L. Crudgington, D. J. Thomson, A. Z. Khokhar, K. Li, W. Cao, G. Z. Mashanovich, and J. Capmany, Nat. Commun. **8**, 636 (2017).
5. Y. Liu, D. Marpaung, A. Choudhary, and B. J. Eggleton, Opt. Lett. **41**, 5306 (2016).
6. M. P. Chang, E. C. Blow, J. J. Sun, M. Z. Lu, and P. R. Prucnal, IEEE Trans. Microw. Theory Tech. **65**, 4493 (2017).
7. A. M. Weiner, Opt. Commun. **284**, 3669 (2011).
8. J. Chang, J. Meister, and P. R. Prucnal, J. Lightwave Technol. **32**, 3623 (2014).
9. T. Ferreira de Lima, A. N. Tait, M. A. Nahmias, B. J. Shastri, and P. R. Prucnal, IEEE Photon. J. **8**, 5500509 (2016).
10. A. N. Tait, T. F. de Lima, E. Zhou, A. X. Wu, M. Chang, M. A. Nahmias, B. J. Shastri, and P. R. Prucnal, *Conference on Lasers and Electro-Optics* (OSA, 2017), paper SM1O.6.
11. A. N. Tait, T. F. de Lima, E. Zhou, A. X. Wu, M. A. Nahmias, B. J. Shastri, and P. R. Prucnal, Sci. Rep. **7**, 7430 (2017).
12. P. R. Prucnal and B. J. Shastri, *Neuromorphic Photonics* (CRC Press, 2017).
13. A. N. Tait, M. A. Nahmias, B. J. Shastri, and P. R. Prucnal, J. Lightwave Technol. **32**, 4029 (2014).
14. A. Tait, T. Ferreira de Lima, M. Nahmias, B. Shastri, and P. Prucnal, IEEE Photon. Technol. Lett. **28**, 887 (2016).
15. A. N. Tait, T. Ferreira de Lima, M. A. Nahmias, B. J. Shastri, and P. R. Prucnal, Opt. Express **24**, 8895 (2016).
16. A. N. Tait, A. X. Wu, T. Ferreira de Lima, E. Zhou, B. J. Shastri, M. A. Nahmias, and P. R. Prucnal, IEEE J. Sel. Top. Quantum Electron. **22**, 5900214 (2016).
17. A. N. Tait, A. X. Wu, T. F. de Lima, M. A. Nahmias, B. J. Shastri, and P. R. Prucnal, *IEEE Photonics Conference (IPC)* (2017), pp. 101–102.
18. E. Klein, D. Geuzebroek, H. Kelderman, G. Sengo, N. Baker, and A. Driessen, IEEE Photon. Technol. Lett. **17**, 2358 (2005).
19. M. S. Dahlem, C. W. Holzwarth, A. Khilo, F. X. Kärtner, H. I. Smith, and E. P. Ippen, Opt. Express **19**, 306 (2011).
20. H. Jayatilleka, K. Murray, M. Caverley, N. Jaeger, L. Chrostowski, and S. Shekhar, J. Lightwave Technol. **34**, 2886 (2015).
21. M. Bahadori, S. Rumley, H. Jayatilleka, K. Murray, N. A. F. Jaeger, L. Chrostowski, S. Shekhar, and K. Bergman, J. Lightwave Technol. **34**, 4043 (2016).
22. O. Schwelb, Proc. SPIE **6343**, 63433P (2006).
23. H. L. Liew and V. Van, J. Lightwave Technol. **26**, 2323 (2008).
24. A. Melloni, Opt. Lett. **26**, 917 (2001).
25. J. E. Heebner, P. Chak, S. Pereira, J. E. Sipe, and R. W. Boyd, J. Opt. Soc. Am. B **21**, 1818 (2004).
26. M. Mancinelli, R. Guider, M. Masi, P. Bettotti, M. R. Vanacharla, J.-M. Fedeli, and L. Pavesi, Opt. Express **19**, 13664 (2011).
27. M. T. Wade and M. A. Popović, Opt. Express **21**, 10903 (2013).
28. I. Chremmos, O. Schwelb, and N. Uzunoglu, *Photonic Microresonator Research and Applications* (Springer, 2010).
29. L. Chrostowski, X. Wang, J. Flueckiger, Y. Wu, Y. Wang, and S. T. Fard, *Optical Fiber Communication Conference* (OSA, 2014), paper Th2A.37.
30. Z. Lu, J. Jhoja, J. Klein, X. Wang, A. Liu, J. Flueckiger, J. Pond, and L. Chrostowski, Opt. Express **25**, 9712 (2017).
31. R. J. Bojko, J. Li, L. He, T. Baehr-Jones, M. Hochberg, and Y. Aida, J. Vac. Sci. Technol. B **29**, 06F309 (2011).
32. "Applied Nanotools NanoSOI process," https://www.appliednt.com/nanosoi/.
33. Y. Wang, X. Wang, J. Flueckiger, H. Yun, W. Shi, R. Bojko, N. A. Jaeger, and L. Chrostowski, Opt. Express **22**, 20652 (2014).
34. J. C. Mikkelsen, W. D. Sacher, and J. K. S. Poon, Opt. Express **22**, 9659 (2014).
35. T. Barwicz, M. A. Popović, M. R. Watts, P. T. Rakich, E. P. Ippen, and H. I. Smith, J. Lightwave Technol. **24**, 2207 (2006).